

A Hashin-Shtrikman type semi-analytical homogenization procedure in multiscale modeling to account for coupled problems

David Jaworek^{1*}, Johanna Waimann¹, Christian Gierden¹, Stephan Wulfinghoff², and Stefanie Reese¹

¹ Institute of Applied Mechanics, RWTH Aachen University, Mies-van-der-Rohe-Str. 1, 52074 Aachen, Germany

² Institute for Material Science, Kiel University, Kaiserstraße 2, 24143 Kiel, Germany

Abstract: Heterogeneous materials are important for a vast amount of applications e.g. in automotive industry or in aerospace. For instance, when producing components, it can be desired to use materials with a heterogeneous microstructure in order to achieve specific material properties. The resulting properties highly depend on the manufacturing process itself, which can involve mechanical and/or thermal loadings. Therefore, it is necessary to properly depict the microstructural material behavior in order to allow for the calibration of the manufacturing process and for the solution of the inverse problem. Constitutive models can be used to depict the material response in a simplified manner. These simplifications allow for a more flexible use of the model but restrict it to a certain range of applications. Thus, it is beneficial to take the material's microscopic structure into account and couple its behavior to the macroscopic response. As multiscale methods (e.g. FE², FE-FFT) are computationally expensive, semi-analytical homogenization procedures are investigated to account for the transition between different length scales. There are various well known homogenization techniques discussed in literature such as e.g. the Voigt and Reuss bounds, the self-consistent method as well as the Mori-Tanaka method. In our presentation, the focus lies on a Hashin-Shtrikman type formulation in similarity with the one proposed by [Wulfinghoff et al. \(2018\)](#). This homogenization technique will then be applied to a heterogeneous elastoplastic material under mechanical and thermal loading. After presenting the homogenized material model, we will proof its applicability by various numerical calculations.

Keywords: Process signatures, heterogeneous material, homogenization, Hashin-Shtrikman, Talbot-Willis, plasticity

1 Introduction

In production engineering the desired material modifications (change of the material properties) highly depend on the chosen process as well as on the chosen process quantities (such as experimental setup, material properties, loading, etc.). For example it is possible to consider processes with different dominant impacts such as mechanical loads (deep rolling, cf. [Meyer et al. \(2011\)](#)), thermal loads (EDM, cf. [Klink et al. \(2011\)](#)), or chemical loads (ECM, cf. [Klocke et al. \(2013\)](#)). However, even for similar processes (e.g. the processes deep rolling and drilling with predominantly mechanical impact) a comparison is often merely impossible due to significantly different boundary conditions. Therefore, material loads have to be derived from the process parameters in order to make different processes comparable. On the one hand, a governing material load could be the strain state inside the material. On the other hand, possible material modifications could be a change of the hardness or a change in the residual stresses. Another problem is linking the material modifications to the process parameters as the direct dependence is usually not known or only known a priori under very special conditions. The term “process signature” describes the interrelation between material loads and material modifications and was established in course of the transregional collaborative research center SFB/TRR 136 (cf. [Brinksmeier et al. \(2011, 2014\)](#)). The idea is depicted in Fig. 1.

For materials with microstructural features (such as steel), these modifications can be measured on either the microscopic or the macroscopic scale. Therefore, it is necessary to employ a strategy to link the two scales. Early works involved procedures such a FE² ([Smit et al. \(1998\)](#); [Feyel \(2003\)](#)). Later, more advanced multi scale approaches as e.g. FE-FFT based methods ([Moulinec](#)

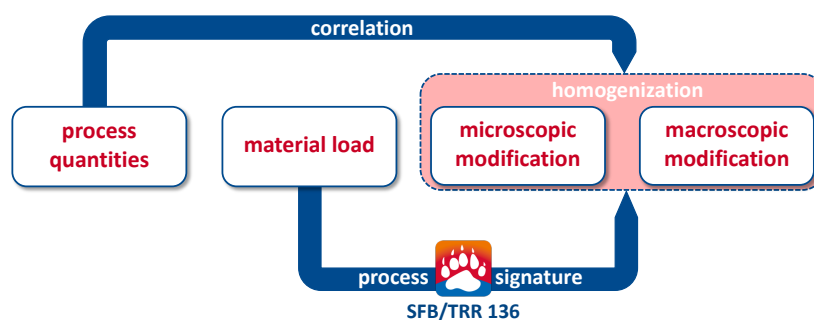


Fig. 1: Schematic sketch of process including process signature.

and Suquet (1995, 1998); Kochmann et al. (2016)) were developed. The range of possible formulations is very wide starting from first order homogenization techniques (Voigt (1889); Reuss (1929)) to more advanced homogenization techniques such as e.g. Mori-Tanaka (Mori and Tanaka (1973)), the self-consistent scheme (Kröner (1958); Hill (1965)), or also Hashin-Shtrikman type formulation (Hashin and Shtrikman (1962a,b)) and Talbot-Willis type method (Willis (1981); Talbot and Willis (1985)). As the process simulations are in general quite complex and hence involve high computational effort, it is necessary to use suitable multi scale approaches. This work deals with the investigation of a Hashin-Shtrikman type homogenization procedure (cf. also Ponte Castaneda and Suquet (1998)) applied for predominantly mechanical processes under isothermal and non-isothermal conditions. In section 2 the Hashin-Shtrikman type homogenization method is presented with application to statistically isotropic elasto-plastic composites. Thereupon, in section 3 different numerical investigations are carried out starting with a Gauss point study for mechanical with and without temperature impact and then continuing with a short Finite element study. Section 4 gives a conclusion and an outlook.

2 Problem Description

The microscopic boundary value problem (BVP) depicted in Fig. 2 is considered. The domain Ω is bounded by $d\Omega$ with prescribed displacements \bar{u} on the Dirichlet boundary $d\Omega_u$ and $div \tau(x)$ acting inside the inhomogeneities. The body is assumed to be statistically isotropic and to consist of randomly distributed ellipsoidal inhomogeneities. Following Eshelby (1957), the inhomogeneities do not interact with each other. This allows for the calculation of the response inside the inhomogeneities separately from the matrix response.

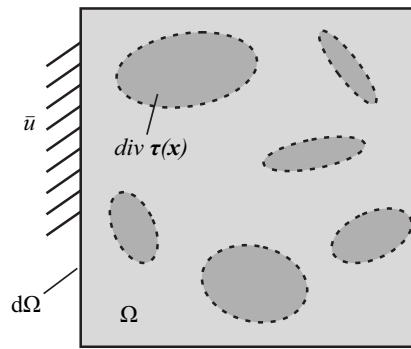


Fig. 2: Heterogeneous BVP.

The strong form of the problem is given by

$$\left. \begin{aligned} \mathbf{0} &= \operatorname{div}(\boldsymbol{\tau} + \mathbb{C}^{(0)} : \boldsymbol{\varepsilon}) \\ \boldsymbol{\tau}(\mathbf{x}, \boldsymbol{\varepsilon}) &= \boldsymbol{\sigma}(\mathbf{x}, \boldsymbol{\varepsilon}) - \mathbb{C}^{(0)} : \boldsymbol{\varepsilon}(\mathbf{x}) \\ \boldsymbol{\sigma}(\mathbf{x}, \boldsymbol{\varepsilon}) &= \mathbb{C}(\mathbf{x}) : \boldsymbol{\varepsilon}(\mathbf{x}) \\ \boldsymbol{\varepsilon}(\mathbf{x}) &= \nabla^{sym} \mathbf{u}(\mathbf{x}) \end{aligned} \right\} \text{in } \Omega, \quad \mathbf{u}(\mathbf{x}) = \bar{\mathbf{u}} = \bar{\boldsymbol{\varepsilon}} \mathbf{x} \text{ on } \partial\Omega, \quad (1)$$

in which the stress $\boldsymbol{\sigma}(\mathbf{x}, \boldsymbol{\varepsilon})$ can involve any elastic or non-elastic constitutive relation. The polarization stress $\boldsymbol{\tau}(\mathbf{x}, \boldsymbol{\varepsilon})$ is the difference between the actual stress field $\boldsymbol{\sigma}(\mathbf{x}, \boldsymbol{\varepsilon})$ and the stress in a homogeneous reference material of stiffness $\mathbb{C}^{(0)}$. The deformations are assumed to be small and the strain field $\boldsymbol{\varepsilon}(\mathbf{x})$ is calculated as the symmetric part of the gradient of the displacement field $\mathbf{u}(\mathbf{x})$. In accordance with Hashin and Shtrikman (1962a,b), the microscopic field quantities are assumed to be phase-wise constant. They can therefore be expressed by

$$\boldsymbol{\sigma}(\mathbf{x}) = \sum_{r=1}^{N_r} \chi^{(r)}(\mathbf{x}) \boldsymbol{\sigma}^{(r)}, \quad \boldsymbol{\varepsilon}(\mathbf{x}) = \sum_{r=1}^{N_r} \chi^{(r)}(\mathbf{x}) \boldsymbol{\varepsilon}^{(r)}, \quad \boldsymbol{\tau}(\mathbf{x}) = \sum_{r=1}^{N_r} \chi^{(r)}(\mathbf{x}) \boldsymbol{\tau}^{(r)}, \quad (2)$$

where any quantity $(\bullet)^{(r)}$ represents the phase-wise constant counterpart of (\bullet) in phase r for which $\mathbf{x} \in \Omega^{(r)}$. Moreover, $\chi^{(r)}(\mathbf{x})$ represents an indicator function which is defined as

$$\chi^{(r)}(\mathbf{x}) = \begin{cases} 1 & \text{if } \mathbf{x} \in \Omega^{(r)} \\ 0 & \text{otherwise} \end{cases}. \quad (3)$$

Combining Eqs. (1) and (2), the microscopical phase-wise constant polarization stress field $\boldsymbol{\tau}^{(r)}$ can be expressed in terms of the phase-wise constant stresses and strains as

$$\boldsymbol{\tau}^{(r)} = \boldsymbol{\sigma}^{(r)}(\boldsymbol{\varepsilon}^{(r)}) - \mathbb{C}^{(0)} : \boldsymbol{\varepsilon}^{(r)}. \quad (4)$$

It is important to mention, that the macroscopic strain field $\bar{\boldsymbol{\varepsilon}}$ is assumed to be constant on the material point level whereas the microscopic strain field $\boldsymbol{\varepsilon}(\mathbf{x})$ is allowed to fluctuate. Utilizing the Lippmann-Schwinger equation (cf. Kröner (1977)), the

microscopic strain field $\boldsymbol{\varepsilon}(\mathbf{x})$ can be calculated by

$$\boldsymbol{\varepsilon}(\mathbf{x}) = \bar{\boldsymbol{\varepsilon}} - \underbrace{\int_{\Omega} \boldsymbol{\Gamma}_{\infty}(\mathbf{x}, \mathbf{x}') : \boldsymbol{\tau}(\mathbf{x}') \, d\mathbf{x}'}_{\tilde{\boldsymbol{\varepsilon}}(\mathbf{x})}. \quad (5)$$

Here, the microscopic strain fluctuation $\tilde{\boldsymbol{\varepsilon}}(\mathbf{x})$ can be obtained by the linear mapping the 2nd order polarization stress field tensor $\boldsymbol{\tau}(\mathbf{x}')$ by the 4th order $\boldsymbol{\Gamma}$ -operator. The $\boldsymbol{\Gamma}$ -operator itself is the second derivative of the Green's function $\boldsymbol{\Gamma}_{\infty}(\mathbf{x}, \mathbf{x}')$ and can be calculated by

$$\boldsymbol{\Gamma}_{\infty}(\mathbf{x}, \mathbf{x}') = \frac{\partial^2 \mathbf{G}_{\infty}(\mathbf{x}, \mathbf{x}')}{\partial \mathbf{x} \partial \mathbf{x}'}. \quad (6)$$

Integrating Eq. (5) over $\Omega^{(r)}$ (the domain of phase r) results in an expression for the average strain field in phase r which reads

$$\boldsymbol{\varepsilon}^{(r)} = \int_{\Omega^{(r)}} \boldsymbol{\varepsilon}(\mathbf{x}) \, d\mathbf{x} = \bar{\boldsymbol{\varepsilon}} - \frac{1}{\lambda^{(r)}} \sum_{s=1}^N \left(\mathbb{E}^{(rs)} : \boldsymbol{\tau}^{(s)} \right). \quad (7)$$

Here, the microstructural tensor $\mathbb{E}^{(rs)}$ describes the interrelation between phases r and s . It is an abbreviation for the volume average over phase r of the convolution integral and reads

$$\mathbb{E}^{(rs)} = \int_{\Omega} \chi^{(r)}(\mathbf{x}) \int_{\Omega} \boldsymbol{\Gamma}_{\infty}(\mathbf{x}, \mathbf{x}') \chi^{(s)}(\mathbf{x}') \, d\mathbf{x}' \, d\mathbf{x}. \quad (8)$$

For the special case of spherical inhomogeneities with an statistically isotropic distribution and a linear elastic reference material, the microstructural tensor simplifies to

$$\mathbb{E}^{(rs)} = \lambda^{(r)} (\delta_{rs} - \lambda^{(s)}) \mathbb{P}^{(0)}, \quad \mathbb{P}^{(0)} = \mathbb{P}^{(0)}(\boldsymbol{\kappa}^{(0)}, \boldsymbol{\mu}^{(0)}) = \text{const}. \quad (9)$$

From Eq. (9), it is apparent, that the microstructural realization does not influence the results as long as the phase fractions are chosen to be constant. In that case $\mathbb{E}^{(rs)}$ solely depends on the phase fractions $\lambda^{(r)}$ as well as on the elastic constants of the homogeneous reference material $\boldsymbol{\kappa}^{(0)}$ and $\boldsymbol{\mu}^{(0)}$.

Hence, for a two-phase composite with volumetric phase fractions $\lambda^{(M)}$ (matrix) and $\lambda^{(I)}$ (inhomogeneities), all microstructural realizations shown in Fig. 3 result in the same macroscopic response when considering the aforementioned simplification.

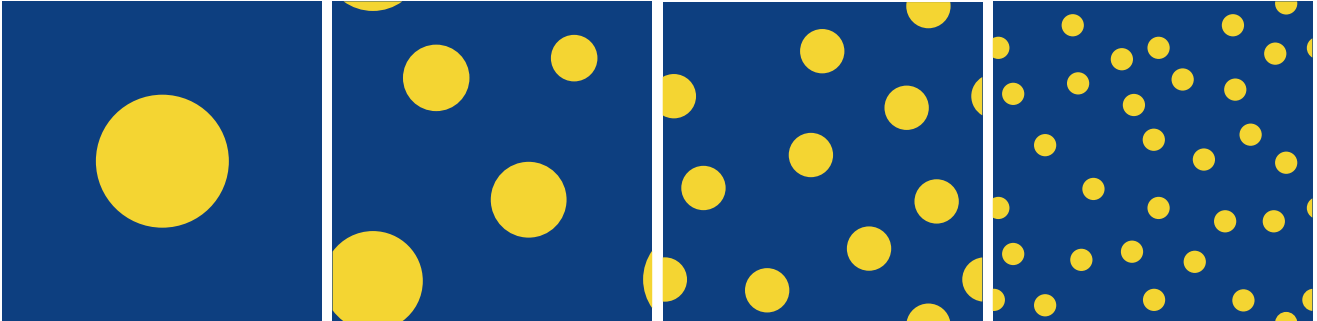


Fig. 3: Different micro structural realizations of same phase fractions.

Subsequently, the microscopic stress and strain tensors $\boldsymbol{\sigma}(\mathbf{x})$ and $\boldsymbol{\varepsilon}(\mathbf{x})$ can be averaged over the volume of the domain by

$$\bar{\boldsymbol{\sigma}} = \int_{\Omega} \boldsymbol{\sigma}(\mathbf{x}) \, d\mathbf{x} = \sum_{r=1}^{N_r} \lambda^{(r)} \boldsymbol{\sigma}^{(r)}, \quad \bar{\boldsymbol{\varepsilon}} = \int_{\Omega} \boldsymbol{\varepsilon}(\mathbf{x}) \, d\mathbf{x} = \sum_{r=1}^{N_r} \lambda^{(r)} \boldsymbol{\varepsilon}^{(r)}, \quad (10)$$

where $\bar{\boldsymbol{\sigma}}$ and $\bar{\boldsymbol{\varepsilon}}$ denote the macroscopical stress and strain tensors.

3 Numerical investigations

3.1 Gauss point study - mechanical loading

In order to evaluate the accuracy of the discussed homogenization procedure, a Gauss point study is carried out. For simplicity, the first realization (cf. Fig. 3) is chosen for carrying out full-field simulations which will then compared with the homogenization procedure. The inclusions are assumed to behave purely elastic. The matrix material is modeled by means of an elasto-plastic constitutive law involving J_2 -plasticity with Voce-type hardening (e.g. as presented in Brepols et al. (2018)). The hardening behavior is described using the yield stress σ_y which is given by

$$\sigma_y = \sigma_{y0} + (\sigma_{y\infty} - \sigma_{y0}) (1 - \exp(-\beta \varepsilon_p^{eq})) \quad (11)$$

in which ε_P^{eq} is the equivalent plastic strain. The elastic and plastic parameters of the matrix as well as the elastic parameters of the inclusions are given in Tab. 1.

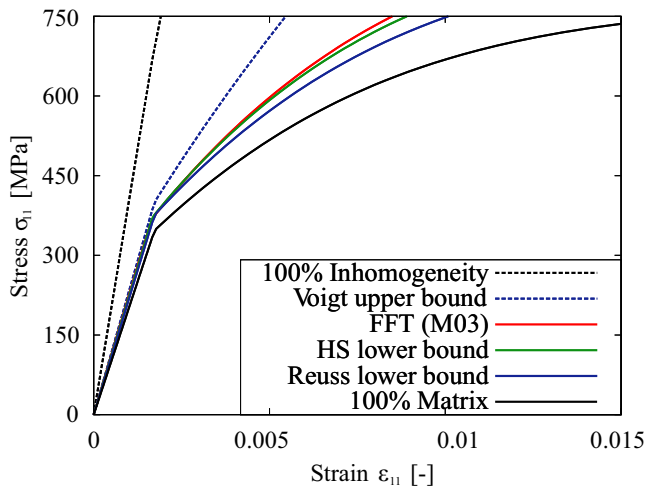
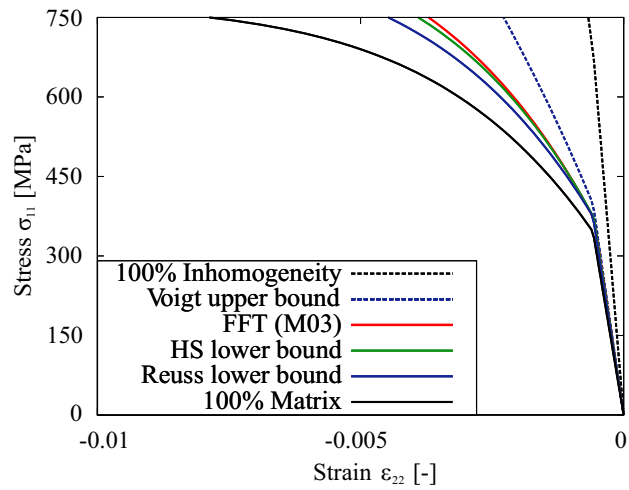
Matrix	Young's modulus $E^{(M)}$	200 GPa
	Poisson's ratio $\nu^{(M)}$	0.34
	Initial yield strength σ_{y0}	350 MPa
	Ultimate strength $\sigma_{y\infty}$	750 MPa
	Hardening parameter β	200
	Volumetric phase fraction $\lambda^{(M)}$	0.85
Inhomogeneities	Young's modulus $E^{(I)}$	400 GPa
	Poisson's ratio $\nu^{(I)}$	0.34
	Volumetric phase fraction $\lambda^{(I)}$	0.15

Tab. 1: Material parameters

A stress-driven computation is carried out with a uniaxial tensile stress of $\sigma_{11} = 750$ MPa. The stress-strain response for the uniaxial strain ε_{11} is shown in Fig. 4, whereas the transversal strain ε_{22} is presented in Fig. 5. As can be observed, the Voigt and Reuss bounds (1st order homogenizations) are compared with the full field solution and the Hashin-Shtrikman lower bound. The error in the strain between the Hashin-Shtrikman homogenization and the full field can be compared for the crucial points $\sigma_{11} = 350$ MPa (yield strength of matrix material) and the final stress of $\sigma_{11} = 750$ MPa. There is no error present for the elastic response whereas the error in the strain ε_{11} for a stress level of $\sigma_{11} = 750$ MPa reads 4.49%. The results are also summarized in Tab. 2.

Method	Run time	Strain ε_{11} at $\sigma_{11} = 350$ MPa	Strain ε_{11} at $\sigma_{11} = 750$ MPa	Error at $\sigma_{11} = 750$ MPa
FFT	89664 s	0.0016	0.0085	4.49%
HS Homogenization	0.012 s	0.0016	0.0089	-

Tab. 2: CPU times and speed-up factors

Fig. 4: Uniaxial tension: σ_{11} vs. ε_{11} .Fig. 5: Uniaxial tension: σ_{11} vs. ε_{22} .

3.2 Gauss point study - mechanical loading with isothermal temperature state

Furthermore, the material response could also be temperature dependent and therefore the elastic and elasto-plastic properties of the microstructure are evolving with temperature change. Considering a steel of type 42CrMo4, the material properties can be taken from literature (e.g. [Miokovic \(2005\)](#)). The Koistinen-Marburger model is used to model phase transformations ([Koistinen and Marburger \(1959\)](#)), where the volumetric phase fraction of the matrix can be calculated by

$$\lambda^{(M)} = \begin{cases} \exp[b(\theta_S - \theta)] & \text{if } \theta < \theta_S \\ 1 & \text{otherwise} \end{cases} \quad (12)$$

In Eq. (12), θ is the current temperature, θ_S is the phase transformation start temperature, and b is a constant that controls the shape of the curve. For $\theta_S = 500^\circ\text{C}$ and $b = -0.01 \frac{1}{^\circ\text{C}}$, the curve looks as shown in Fig. 6.

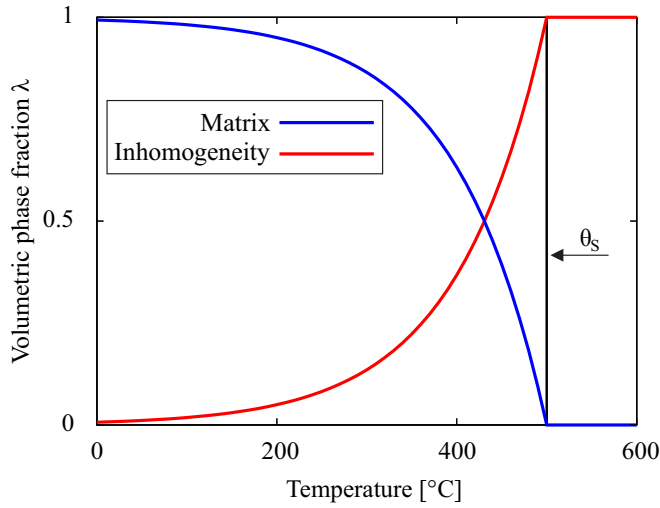


Fig. 6: Temperature induced phase transformation.

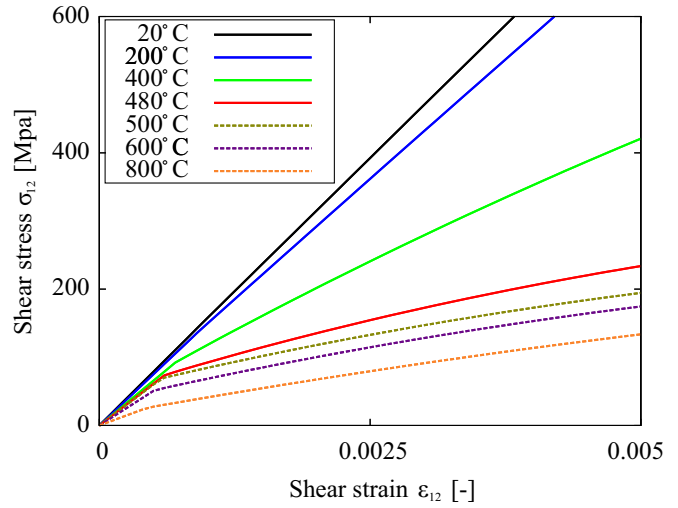


Fig. 7: Temperature dependent results for isothermal loading.

Now, the homogenization method can be evaluated again for different isothermal temperature states. As can be observed in Fig. 7, the overall response is linear elastic for low temperatures as the specimen then only consists of the linear elastic inhomogeneity material. For increasing temperatures, the response becomes softer until we reach a fully elasto-plastic response for temperatures over 500 °C which is the temperature at which the phase transformation is completed and only matrix material is present.

3.3 Finite Element study - mechanical loading for non-isothermal temperature states

Further, a simple tensile experiment can be calculated using the Finite Element Analysis Program (FEAP) (Taylor (2014)) where the procedure has been implemented as a user material routine (UMAT).

The structure is symmetric with respect to its geometry and loading in all directions and therefore only $\frac{1}{8}$ of the specimen size is used.

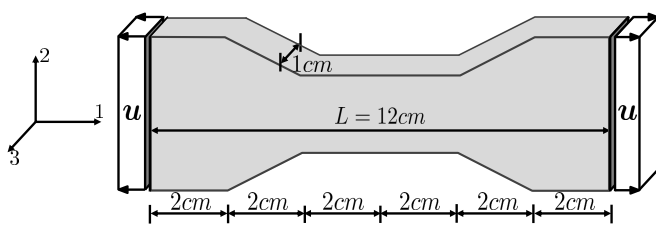


Fig. 8: Schematic view of the 3D tensile specimen.

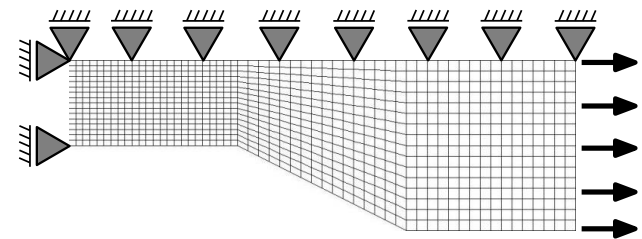


Fig. 9: Reduced mesh involving symmetric BCs.

In order to take a very weak one-directional thermal coupling into account, the material parameters are set to be temperature dependent as described in section 3.2.

Applying a gradually increasing displacement u until reaching $u_{max} = 0.02 L = 0.24$ cm, while decreasing the temperature from 600 °C to 20 °C, the evolution of the von Mises stresses over time can be measured for different integration points. The phase transformation sets in as soon as reaching the phase transformation start temperature $\theta_s = 500$ °C (cf. Figs. 6 and 10).

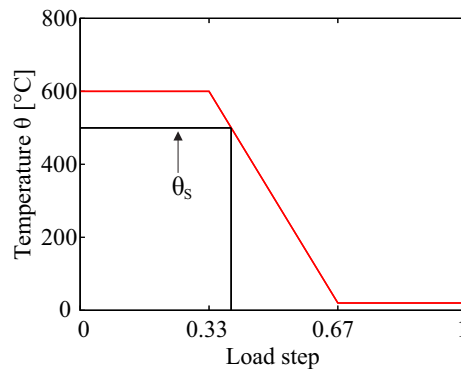


Fig. 10: Temperature load.

Fig. 11 illustrates the evolution of the von Mises stress σ_v over time for three points in the specimen. Furthermore, the von Mises stress distribution over time is shown for the last step.

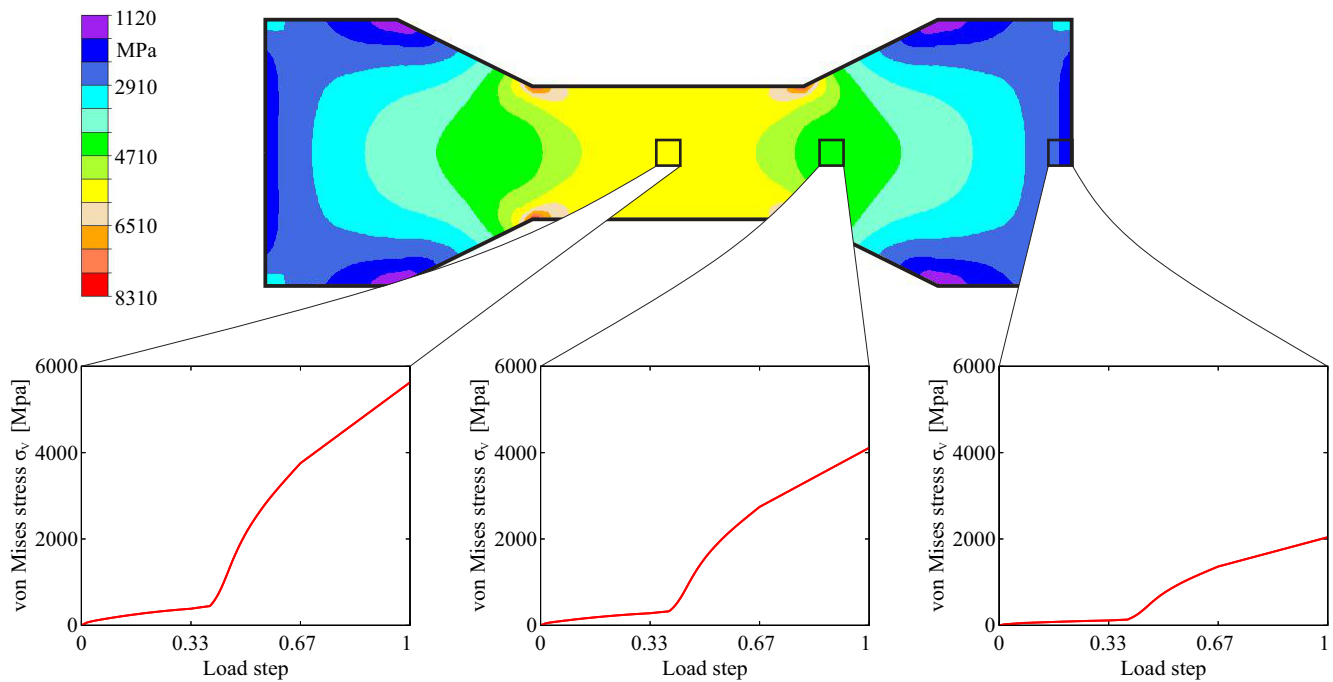


Fig. 11: Finite element simulation results.

In the beginning the specimen only consists of matrix material and thus behaves elasto-plastically for temperatures higher than 500 °C. With decreasing temperature the response becomes stiffer as the material stiffness increases and as the phase transformation sets in. When reaching very low temperatures (here 20 °C), the specimen nearly only consists of linear elastic inhomogeneity and therefore the response is purely elastic.

4 Conclusions and Outlook

The presented homogenization framework following the procedure by Hashin and Shtrikman and incorporating the developments by Talbot and Willis allows for the computation of elasto-plastic composites under small strains. The results obtained are in good agreement with the reference solution provided by FE-FFT simulations. One assumption is the statistically isotropic distribution of the spherical inhomogeneities which simplifies the computation of the microstructural tensor $\mathbb{E}^{(r,s)}$. It is shown, that the method can be applied for mechanical calculations under isothermal or non-isothermal conditions.

As the simplification of a statistically isotropic microstructure with spherical inclusions is very limiting, further research should tackle this problem and take more complex micro structural distributions into account. This could be achieved incorporating a more elaborate approach for the calculation of $\mathbb{E}^{(r,s)}$. Moreover, in order to simulate thermal processes properly, a consistent thermo-mechanical coupling is to be developed and coupled with the homogenization procedure. Further, a more profound model for capturing the microstructural evolution of the phases should be considered when investigating thermal or thermo-mechanical processes. One possible approach would be incorporating a phase transformation model based on variational methods (cf. e.g. Carstensen et al. (2002); Hackl and Fischer (2008); Junker et al. (2014)).

Acknowledgements

The work is funded by the Deutsche Forschungsgemeinschaft (DFG, German Research Foundation) - Projektnummer 223500200 - TRR 136. We gratefully acknowledge the financial support of the subprojects M05 and M03.

References

- T. Brepols, S. Wulfinghoff, and S. Reese. *A Micromorphic Damage-Plasticity Model to Counteract Mesh Dependence in Finite Element Simulations Involving Material Softening*, pages 235–255. Springer International Publishing, Cham, 2018. doi: https://doi.org/10.1007/978-3-319-65463-8_2.
- E. Brinksmeier, R. Gläbe, F. Klocke, and D.A. Lucca. Process signatures - an alternative approach to predicting functional workpiece properties. *Procedia Engineering*, 19:44 – 52, 2011. ISSN 1877-7058. doi: <https://doi.org/10.1016/j.proeng.2011.11.078>. 1st CIRP Conference on Surface Integrity (CSI).
- E. Brinksmeier, F. Klocke, D. A. Lucca, J. Sölter, and D. Meyer. Process signatures - a new approach to solve the inverse surface integrity problem in machining processes. *Procedia CIRP*, 13:429–434, 2014. doi: <https://doi.org/10.1016/j.procir.2014.04.073>.
- C. Carstensen, K. Hackl, and A. Mielke. Non-convex potentials and microstructures in finite-strain plasticity. *Proc. R. Soc. Lond. A*, 458:299–317, 2002. doi: <https://doi.org/10.1098/rspa.2001.0864>.
- J. D. Eshelby. The determination of the elastic field of an ellipsoidal inclusion, and related problems. *Proceedings of the Royal Society of London A*, 241(1226):376–396, 1957. doi: <https://doi.org/10.1098/rspa.1957.0133>.

- F. Feyel. A multilevel finite element method (fe2) to describe the response of highly non-linear structures using generalized continua. *Computer Methods in Applied Mechanics and Engineering*, 192(28):3233 – 3244, 2003. ISSN 0045-7825. doi: [https://doi.org/10.1016/S0045-7825\(03\)00348-7](https://doi.org/10.1016/S0045-7825(03)00348-7). Multiscale Computational Mechanics for Materials and Structures.
- K. Hackl and F. D. Fischer. On the relation between the principle of maximum dissipation and inelastic evolution given by dissipation potentials. *Proceedings of the Royal Society A*, 464:117–132, 2008. doi: <https://doi.org/10.1098/rspa.2007.0086>.
- Z. Hashin and S. Shtrikman. On some variational principles in anisotropic and nonhomogeneous elasticity. *Journal of the Mechanics and Physics of Solids*, 10(4):335–342, 1962a. doi: [https://doi.org/10.1016/0022-5096\(62\)90004-2](https://doi.org/10.1016/0022-5096(62)90004-2).
- Z. Hashin and S. Shtrikman. A variational approach to the theory of the elastic behaviour of polycrystals. *Journal of the Mechanics and Physics of Solids*, 10(4):343–352, 1962b. doi: [https://doi.org/10.1016/0022-5096\(62\)90005-4](https://doi.org/10.1016/0022-5096(62)90005-4).
- R. Hill. A self-consistent mechanics of composite materials. *Journal of the Mechanics and Physics of Solids*, 13(4):213 – 222, 1965. ISSN 0022-5096. doi: [https://doi.org/10.1016/0022-5096\(65\)90010-4](https://doi.org/10.1016/0022-5096(65)90010-4).
- P. Junker, J. Makowski, and K. Hackl. The principle of the minimum of the dissipation potential for non-isothermal processes. *Continuum Mechanics and Thermodynamics*, 26(3):259–268, May 2014. doi: <https://doi.org/10.1007/s00161-013-0299-4>.
- A. Klink, Y.B. Guo, and F. Klocke. Surface integrity evolution of powder metallurgical tool steel by main cut and finishing trim cuts in wire-edm. *Procedia Engineering*, 19:178–183, 12 2011. doi: [10.1016/j.proeng.2011.11.098](https://doi.org/10.1016/j.proeng.2011.11.098).
- F. Klocke, M. Zeis, S. Harst, A. Klink, D. Veselovac, and M. Baumgaertner. Modeling and simulation of the electrochemical machining (ecm) material removal process for the manufacture of aero engine components. *Procedia CIRP*, 8:265 – 270, 2013. ISSN 2212-8271. doi: <https://doi.org/10.1016/j.procir.2013.06.100>. 14th CIRP Conference on Modeling of Machining Operations (CIRP CMMO).
- J. Kochmann, S. Wulfinghoff, S. Reese, J. R. Mianroodi, and B. Svendsen. Two-scale fe-fft- and phase-field-based computational modeling of bulk microstructural evolution and macroscopic material behavior. *Computer Methods in Applied Mechanics and Engineering*, 305:89 – 110, 2016. ISSN 0045-7825. doi: <https://doi.org/10.1016/j.cma.2016.03.001>.
- D.P. Koistinen and R.E. Marburger. A general equation prescribing the extent of the austenite-martensite transformation in pure iron-carbon alloys and plain carbon steels. *Acta Metallurgica*, 7(1):59 – 60, 1959. ISSN 0001-6160. doi: [https://doi.org/10.1016/0001-6160\(59\)90170-1](https://doi.org/10.1016/0001-6160(59)90170-1).
- E. Kröner. Berechnung der elastischen konstanten des vielkristalls aus den konstanten des einkristalls. *Zeitschrift für Physik*, 151 (4):504–518, Aug 1958. doi: <https://doi.org/10.1007/BF01337948>.
- E. Kröner. Bounds for effective elastic moduli of disordered materials. *Journal of the Mechanics and Physics of Solids*, 25(2): 137–155, 1977. doi: [https://doi.org/10.1016/0022-5096\(77\)90009-6](https://doi.org/10.1016/0022-5096(77)90009-6).
- D. Meyer, E. Brinksmeier, and F. Hoffmann. Surface hardening by cryogenic deep rolling. *Procedia Engineering*, 19:258 – 263, 2011. ISSN 1877-7058. doi: <https://doi.org/10.1016/j.proeng.2011.11.109>. 1st CIRP Conference on Surface Integrity (CSI).
- T. Miokovic. *Analyse des Umwandlungsverhaltens bei ein- und mehrfacher Kurzzeithärtung bzw. Laserstrahlhärtung des Stahls 42CrMo4*. PhD thesis, 2005. URL <https://publikationen.bibliothek.kit.edu/1000003805>.
- T. Mori and K. Tanaka. Average stress in matrix and average elastic energy of materials with misfitting inclusions. *Acta Metallurgica*, 21(5):571 – 574, 1973. ISSN 0001-6160. doi: [https://doi.org/10.1016/0001-6160\(73\)90064-3](https://doi.org/10.1016/0001-6160(73)90064-3).
- H. Moulinec and P. Suquet. A fft-based numerical method for computing the mechanical properties of composites from images of their microstructure. *Microstructure-Property Interactions in Composite Materials*, pages 235–246, 1995. doi: https://doi.org/10.1007/978-94-011-0059-5_0.
- H. Moulinec and P. Suquet. A numerical method for computing the overall response of nonlinear composites with complex microstructure. *Computer Methods in Applied Mechanics and Engineering*, 157(1):69 – 94, 1998. ISSN 0045-7825. doi: [https://doi.org/10.1016/S0045-7825\(97\)00218-1](https://doi.org/10.1016/S0045-7825(97)00218-1).
- P. Ponte Castaneda and P. Suquet. Nonlinear composites. *Advances in Applied Mechanics*, 34:171–302, 1998. doi: [https://doi.org/10.1016/S0065-2156\(08\)70321-1](https://doi.org/10.1016/S0065-2156(08)70321-1).
- A. Reuss. Berechnung der fließgrenze von mischkristallen auf grund der plastizitätsbedingung für einkristalle. *Zeitschrift fuer angewandte Mathematik und Mechanik*, 9:49–59, 1929. doi: <https://doi.org/10.1002/zamm.19290090104>.
- R. J. M. Smit, W. A. M. Brekelmans, and H. E. H. Meijer. Prediction of the mechanical behavior of nonlinear heterogeneous systems by multi-level finite element modeling. *Computer Methods in Applied Mechanics and Engineering*, 155(1):181 – 192, 1998. ISSN 0045-7825. doi: [https://doi.org/10.1016/S0045-7825\(97\)00139-4](https://doi.org/10.1016/S0045-7825(97)00139-4).
- D. R. S. Talbot and J. R. Willis. Variational principles for inhomogeneous nonlinear media. *IMA Journal of Applied Mathematics*, 35(4b):39–54, 1985. doi: <https://doi.org/10.1093/imamat/35.1.39>.
- R. L. Taylor. FEAP - finite element analysis program, 2014. URL <http://www.ce.berkeley/feap>.
- W. Voigt. Ueber die beziehung zwischen den beiden elasticitätsconstanten isotroper körper. *Annalen der Physik*, 38:573–587, 1889. doi: <https://doi.org/10.1002/andp.18892741206>.
- J. R. Willis. Variational and related methods for the overall properties of composites. *Advances in Applied Mechanics*, 21:1–78, 1981. doi: [https://doi.org/10.1016/S0065-2156\(08\)70330-2](https://doi.org/10.1016/S0065-2156(08)70330-2).
- S. Wulfinghoff, F. Cavaliere, and S. Reese. Model order reduction of nonlinear homogenization problems using a hashin-shtrikman type finite element method. *Computer Methods in Applied Mechanics and Engineering*, 330(1):149–179, 2018. doi: <https://doi.org/10.1016/j.cma.2017.10.019>.